Damping Mechanisms of Piezoelectric Quartz Tuning Forks Employed in Photoacoustic Spectroscopy for Trace Gas Sensing

Marilena Giglio, Giansergio Menduni, Pietro Patimisco, Angelo Sampaolo, Arianna Elefante, Vittorio M. N. Passaro, and Vincenzo Spagnolo*

A study of the dependence of main loss mechanisms on the geometry of piezoelectric quartz tuning forks (QTFs) is reported. The influence of these loss mechanisms on the quality factor Q occurring while the QTF vibrates at the in-plane flexural fundamental and first overtone resonance modes is investigated. From this study, two QTFs efficiently operating both at the fundamental and first overtone mode are designed and realized. Data analysis demonstrates that air viscous damping is the dominant energy dissipation mechanism for both flexural modes. However, at the first overtone mode the air damping is reduced and higher quality factors can be obtained when operating at the first overtone mode with respect to the fundamental one.

1. Introduction

Piezoelectric quartz tuning forks (QTFs) are cheap, commercially available, and high-quality resonators. They are widely used as the main component for timekeeping in watches and frequency measurements. Typically, the QTF prongs have a rectangular shape, few millimeters long, and a fraction of a millimeter wide. Used for time measurement applications, they usually operate at a frequency of 2^{15} Hz ≈ 32.7 kHz. QTFs are driven into oscillation by applying an alternating voltage to the gold pads deposited on both prongs. Exploiting the piezoelectric effect occurring in quartz, a charge displacement occurs on prong surface as the prongs bend, leading to the generation of a piezoelectric current proportional to the amplitude of the exciting voltage.[1] Recently, the use of QTFs has been extended to other applications, such as atomic force

microscopy,[2–4] photoacoustic gas sensing,[5–7] rheology,[8] and high-resolution accelerometer and gyroscopes measurements.[9] In quartz-enhanced photoacoustic spectroscopy (QEPAS) the QTF is immersed in a low-pressure gas and a laser beam is focused between the two prongs. The gas absorbing the laser light relaxes via non-radiative molecular collisions, causing a temperature increase and thus a gas expansion. If the laser is modulated at one of frequencies of the in-plane flexural resonance modes, non-radiative relaxation processes generate sequential gas expansion, generating weak pressure waves (i.e., sound) that hit and bend QTF prongs. A QEPAS sensor performance depends on the selected QTF resonance quality factor Q, which is the ratio of the total input energy into the resonator to the energy dissipated within a vibration cycle.[10] A high-quality factor indicates a small resonance bandwidth and low dissipation losses. To improve the design of these devices, it is important to know which factors contribute to the energy dissipation processes. Several QTFs geometries have been proposed for QEPAS, with resonance frequency spanning from 2.8 to 32 kHz for the fundamental flexural mode.[10–13] By lowering the fundamental resonance mode below 5 kHz, the first overtone mode (having a frequency about x6 larger than the fundamental one) also become suitable for QEPAS sensing.[14–17] In a QTF, fundamental and first overtone modes exhibit substantially different resonance properties, mainly because loss mechanisms are strongly dependent on the related vibrational dynamics.

In this work, we identify the two main loss mechanisms occurring in a QTF vibrating at the fundamental and the overtone mode. Starting from theoretical models describing each loss mechanism, two QTF geometries optimized to operate efficiently both at the fundamental and at the first overtone mode have been designed, realized, and tested. The resonance properties, namely the resonance frequency and the quality factor, were measured at atmospheric pressure as well as at 25 Torr.

2. Loss Mechanisms

In the Euler–Bernoulli beam theory, each vibrating prong of a QTF can be treated as a single cantilever, that is, the coupling between them is neglected. The model allows the calculation of the discrete infinite natural resonance frequencies f_n for in-plane

Dr. M. Giglio, Dr. G. Menduni, Dr. P. Patimisco, Dr. A. Sampaolo, Dr. A. Elefante, Prof. V. Spagnolo
PolySense Lab – Dipartimento Interateneo di Fisica
Politecnico and University of Bari
Via Amendola 173, Bari, Italy
E-mail: vincenzoluigi.spagnolo@poliba.it

Prof. V. M. N. Passaro
Photonics Research Group
Dipartimento di Ingegneria Elettrica e dell'Informazione,
Politecnico of Bari
Via Orabona 4, Bari 70126, Italy

**ADVANCED
SCIENCE NEWS**

www.advancedsciencenews.com

**physica
status
solidi a**

www.pss-a.com

flexural modes, given by[18]:

$$f_n = \frac{\pi T}{8\sqrt{12}L^2} \sqrt{\frac{E}{\rho} m_n^2} \qquad (1)$$

where $E = 0.72 \cdot 10^{11} \,\mathrm{N\,m^{-2}}$ and $\rho = 2650 \,\mathrm{Kg\,m^{-3}}$ are the quartz Young's modulus and the quartz density, respectively. T is the prong thickness, L its length and m_n is the mode number. The lowest resonance mode is usually referred to as the fundamental one ($m_0 = 1.194$), while subsequent ones are called overtone modes ($m_1 = 2.998$ for the first overtone mode).

When vibrating prongs undergo harmonic oscillations of small amplitude in a gas, they tend to induce particle motion in the fluid, giving rise to energy loss and additional inertia. By adding to Euler–Bernoulli equation both a resistive part, which takes into account the energy dissipation by acoustic loss, and a reactive part which is responsible of additional inertia to the prong, a linear increase of the resonance frequency is predicted when the pressure is reduced.[18] However, the influence of the air damping on the resonance quality factor cannot be treated by using the Euler–Bernoulli theory. In addition, the so-called support loss mechanism related to mechanical energy transfer from the vibrating prong to the support must be taken into account.[19] Air damping is referred to as an extrinsic loss mechanism, while support damping is considered an intrinsic loss mechanism. Both these loss mechanisms strongly depend on prongs size and the dynamic of the vibrational mode under consideration. Several theoretical models have been proposed for each loss mechanism and their dependence on the main physical parameters have been reported. Each loss contribution is independent from the other, but all concur simultaneously to determine the QTF resonances quality factors.

2.1. Air Damping

When a QTF vibrating prong is immersed in air, a drag force is exerted on it. This force is proportional to the local velocity of the prong in terms of the damping parameter C_{air}. The damping parameter allows calculating the mechanical quality factor of the damped system. Since C_{air} is pressure-dependent, three pressure regions can be identify, each characterized by a different dominant damping mechanism: intrinsic, molecular, and viscous region. In the intrinsic region, the fluid pressure is so low that the damping is negligible compared to the intrinsic damping of the vibrating beam itself. Hence, the Q-factor is independent on the fluid pressure. In the molecular region, damping is caused by independent collisions of non-interacting molecules with the vibrating beam. In this case, the drag force can be determined by employing the kinetic theory of gases, leading to a damping parameter C_{air} proportional to the fluid pressure and the beam geometry. In the viscous region, the medium acts as a viscous fluid and the drag force is calculated using fluid mechanics. W. E. Newell derived an expression for the critical pressure p_c at which the air damping changes from molecular to viscous region, $p_c = 0.3\,\mathrm{Torr\,w^{-1}}$, where w is the crystal width expressed in millimeters.[20] With $0.25\,\mathrm{mm} < w < 0.5\,\mathrm{mm}$, p_c is $<1.2\,\mathrm{Torr}$. Since QEPAS sensors operate at

higher pressure, in all cases reported in this manuscript the QTFs operate in the viscous region. Starting from these assumptions, Blom et al.[21] derived an analytical expression for both the total mechanical energy of the vibrating beam and the dissipated energy per period, leading to a formulation of quality factor related to fluid damping (Q_{air}):

$$Q_{air} = \frac{2\pi\rho Twf_n}{C_{air}} \qquad (2)$$

Q_{air} does not depend on the vibrating mode shape and has the same expression for each vibrational mode. Hosaka et al.[22] have proposed an approximation for the air damping problem of a vibrating prong. Kokubun et al.[23] considered each prong of the QTF having a rectangular cross-section acting as a string of spheres. If these spheres vibrate independently of each other, the resulting drag force is the sum of the drag force of each single sphere. Starting from this approximation, Hosaka et al.[22] made two assumptions: 1) the length L of the QTF prong is much greater than its thickness T and crystal width w and 2) every single portion of the beam is replaced with a sphere of diameter w. They derived an expression for C_{air} and a formulation of Q_{air} given by:

$$Q_{air} = \frac{4\pi\rho Tw^2 f_n}{3\pi\mu w + \frac{3}{4}\pi w^2 \sqrt{4\pi\rho_{air}\mu f_n}} \qquad (3)$$

where ρ_{air} is the air density and μ its viscosity. Losses due to the air damping, proportional to the reciprocal of Q_{air}, consist of two terms: one pressure-independent (assuming a negligible dependence of f_n on the air pressure) and the other one pressure-dependent. $\rho_{air} = MP/R\theta$ is estimated by using the ideal gas law, where $M = 28.964\,\mathrm{kg\,mol^{-1}}$ is the molar mass, $R = 62.3637\,\mathrm{m^3 \cdot Torr/K \cdot mol}$ is the gas constant and θ (in K) is the prong temperature. Q_{air} depends on the air pressure as well as on the resonance frequency and the prong sizes and decreases rapidly when the pressure increases. At higher pressures, Q_{air} levels off and becomes quasi-asymptotic at atmospheric pressure.

The air damping mechanisms are strongly reduced for higher order vibrational modes. For example, at atmospheric pressure, Q_{air} is three times higher for the first overtone mode with respect to the fundamental mode. By combining Equations (1) and (3), an explicit dependence of Q_{air} can be derived as a function of the prong size.[24] The guideline that emerges from this model is that to reduce viscous losses the T/L ratio must be kept high. In addition, the lower the crystal thickness, the higher the air damping losses.

2.2. Support Losses

Although the history of support losses can be tracked back to the 1960s, this field still requires improved models to quantify these loss mechanisms. Models describing support losses have been developed using the theory of elasticity taking into account the beam dynamics and stress-wave propagation. Several models have been developed to analyse support losses and all of them share the following set of assumptions: 1) elastic waves are

transmitted to the support form the vibrating shear forces induced by the oscillating beam with a fixed end; 2) energy propagating through the support does not reflect back into the resonator; and 3) the prong-support junction section is assumed to have zero-displacement.[25–27] The simplest model was developed by Hao et al.[26] in which the prong is supposed to be a rectangular cross-section resonator, attached monolithically to a larger support with the same thickness as that of the prong. The crystal thickness w is assumed to be much smaller than the elastic wavelength λ of the propagating waves. The closed-form expression for the quality factor related to the support losses in a clamped-free cantilever can be expressed as:

$$Q_{\sup p} = A_n \frac{L^3}{T^3} \tag{4}$$

with A_n coefficients depending on the resonance mode number and the prong material. Hao et al. estimated $A_0 = 2.081$ for the fundamental mode and $A_1 = 0.173$ for the first overtone mode. Other models were developed, all of them agreeing on the support losses $(L/T)^3$ dependence but differing in the coefficient values.[25–27] In **Table 1**, theoretical models for Q_{supp} prediction are summarized, with a highlight on the prong geometry dependence and on main hypotheses assumed in the theoretical models. D. Photiadis and J. Judge[25] predict a different prong geometry dependence with respect to the other two models, but an explicit dependence on the resonance mode is not provided. For this reason, it cannot be used in the present work. From these models, the straightforward approach for reducing support losses is designing QTFs having prongs with large length-to-thickness aspect ratios. Higher order modes suffer from higher support losses according to Equation (4). Indeed, an increase of about a factor of 10 on support losses is expected, when changing from the QTF fundamental to its first overtone mode. The influence of support losses on resonance mode order can be explained by using the Euler–Bernoulli beam theory, which allows a derivation of the mode shape of in-plane flexural modes. The fundamental in-plane flexural mode is characterized by a single antinode point on the prong tip, while the first overtone mode has an additional antinode point located at the half of the

prong length.[10] For the first overtone mode, the second antinode causes a higher stress on the QTF support and hence an increase of the support losses with respect to the fundamental mode. The mode shape and the antinode positions were experimentally investigated by using QEPAS. In this technique, a modulated laser light is focused between the QTF prongs. By moving the laser spot along the QTF axis, a QEPAS signal proportional to the induced deformation on the QTF prong can be recorded as a function of the laser beam position. A good agreement was found between the Euler–Bernoulli's prediction and the QEPAS measurement.[10]

3. Tuning Fork Design for Quartz-Enhanced Photoacoustic Spectroscopy

In QEPAS operation, the tuning fork is used as acoustic transducer to convert sound waves produced by an absorbing gas in an electrical signal. The sound wave generation efficiency is strictly related to the capability of the gas to completely relax the excess of energy before the succeeding light absorption process occurs.[28–30] This means that the sound wave generation efficiency is mainly determined by the resonance frequency of the vibrating QTF mode. In QEPAS, the operating frequency should not exceed 40 kHz to ensure that the transfer of the excess energy absorbed by the target gas follows efficiently the fast modulation of the incident laser radiation.[5] It was also demonstrated that lowering the resonance frequency is beneficial for QEPAS sensing.[31] This establishes the main constraint in the realization of QTFs to be used as acoustic transducer in QEPAS both at fundamental and first overtone flexural mode.

For the investigation proposed in this work, the first overtone resonance frequency is fixed to ≈20 kHz: in this way, by using the Euler–Bernoulli equation, the fundamental mode resonance falls at ≈3 kHz. Lowering the operating frequency at values <3 kHz is not recommended in QEPAS since the sensor system would be more influenced by the environmental acoustic noise. According to Equation (1), this constraint on the resonance frequency leads to the length and the thickness of the prongs to be fixed by the relation $T/L^2 \approx 3.8 \cdot 10^{-3}$ in mm^{-1} units. This condition must be combined with practical requirements. When the QTF is excited both at the fundamental and the first overtone mode in QEPAS, one laser beam is focused close to the antinode point of the fundamental mode, which is located at the top of the QTF, while the second laser beam is focused close to the second antinode point of the overtone mode, located close to the middle of prong.[15,16] Hence, for practical use, the prong length should be not less than 0.5 cm. In addition, a constraint can be fixed also on the prong thickness T: QTFs are realized via standard chemical etching and when $T < 300\,\mu m$ imperfections can affect both the geometry and the symmetry of two prongs. All combinations of prong thickness and length satisfying these requirements were simulated. A precision of 1.0 and 0.1 mm was assumed for the prong length and thickness, respectively. Q_{air} and Q_{supp} values were calculated by using Equations (3) and (4), respectively, assuming a crystal thickness of 0.25 mm. The results are reported in **Table 2**.

For both the fundamental and the first overtone mode, the air damping strongly decreases at longer prongs while the support

Table 1. Theoretical models proposed in literature for the prediction of Q_{supp} as a function of the QTF prong geometry. The main assumptions adopted for the models are also reported.

Model [reference]	Q_{supp} prediction	Main assumptions
Jimbo and Itao[19]	$Q_{supp} \propto \frac{L^3}{T^3}$	• 2D wave theory • Semi-infinite elastic support • Fixed ends have zero displacement
Hao, et al.[26]	$Q_{supp} = A_n \frac{L^3}{T^3}$	• 2D wave theory • Beam and support have same width • $\lambda \gg w$ • No displacement or velocity at fixed ends • Dissipation through shear force
D. Photiadis and J. Judge[25]	$Q_{supp} \approx \frac{1}{0.31} \frac{L}{w} \frac{L^4}{T^4}$	• Semi elastic medium • Only shear force was applied while torque was considered negligible

Table 2. Calculated f_0, f_1, and related Q_{air} and Q_{supp} values for QTFs having prong length L spanning from 10 and 19 mm with related prong thickness T properly chosen to ensure a fundamental mode resonance frequency 3.2 kHz $< f_0 <$ 3.5 kHz and first overtone resonance frequency 19 kHz $< f_1 <$ 22 kHz, estimated by using Equation (1). Q_{air} and Q_{supp} are calculated by using Equations (3) and (4), respectively.

L [mm]	T [mm]	Fundamental mode			First overtone mode		
		f_0 [Hz]	Q_{air}	Q_{supp}	f_1 [Hz]	Q_{air}	Q_{supp}
10	0.4	3367.91	10 894	56 187	19 529.44	31 820	4671
11	0.5	3479.25	15 232	32 516	21 091.79	44 277	2703
12	0.6	3508.24	19 425	22 158	21 789.04	56 352	1842
13	0.7	3487.48	23 429	16 648	21 970.62	67 933	1384
14	0.8	3436.65	27 234	13 329	21 840.62	78 996	1108
15	0.9	3367.91	30 845	11 153	21 522.24	89 550	927
16	1.0	3288.98	34 272	9634	21 091.79	99 624	801
17	1.0	3204.76	37 527	8524	20 597.46	109 248	709
18	1.2	3378.31	40 624	7681	20 070.05	118 456	639
19	1.4	3265.29	49 598	5524	21 156.89	144 147	459
20	1.6	3367.91	52 304	5202	20 449.11	152 336	432

loss increases. As discussed in the previous section, theoretical models describe each loss mechanism as standalone. To investigate which loss mechanism dominates, we selected two different QTF geometries from Table 2: the first having $L = 11$ mm, $T = 0.5$ mm (named hereafter as QTF#1) and the second with a longer prong length, $L = 17$ mm, $T = 1$ mm (named hereafter as QTF#2), both with a crystal thickness $w = 0.25$ mm. A schematic of these QTFs is shown in **Figure 1**. Both QTFs were realized starting from a z-cut quartz wafer with a 2° rotation along the x-axis. The geometry was generated by chemical etching and electrodes, consisting of chromium (50 Å thick) and gold (250 Å thick) patterns, were applied photolithographically by means of shadow masks defined on both sides of the wafer. The electrode pattern was designed to enhance the fundamental flexural mode but allowing also the excitation of the first overtone mode.[24]

4. Measurement of Resonance Properties

The properties of a QTF, namely the resonance frequency and the quality factor, can be measured by exciting it electrically. A sketch of the experimental setup is depicted in **Figure 2**. A sinusoidal voltage excitation results in a piezoelectric charge distribution across the QTF prongs. This piezoelectric current is then converted to a voltage signal by means of a custom-made trans-impedance pre-amplifier. The voltage signal is then fed to a lock-in amplifier to be demodulated at the same frequency of the signal excitation. The QTF was mounted in a vacuum chamber, connected with a pressure controller and an oil-free pump in order to keep fixed the working pressure. The QTF response curves were acquired by performing a wide frequency scan of the excitation voltage. Since the air damping losses are dependent on the air pressure surrounding the QTF, the QTF response curves were acquired both at atmospheric pressure and at 25 Torr. The resonance curves measured for QTF#1 and QTF#2 at atmospheric pressure, both for the fundamental and overtone mode, are shown in **Figure 3**.

Each spectral response was fitted by using a Lorentzian function to determine the resonance frequency, that is, the peak frequency value f of the Lorentzian fit function, and the full-width-half-maximum (FWHM). The FWHM value allow determining the quality factor as $Q = f$/FWHM for the fundamental and overtone mode. In **Table 3**, the resonance frequencies and quality factors are reported for both resonance modes, at atmospheric pressure. Discrepancies between the calculated and measured resonance frequency can be mainly ascribed to: 1) gas damping; 2) additional weight of the electrode gold layers; 3) dependence of the elasticity modulus of quartz on the crystallographic axes orientation; 4) deviations in geometry between the modeled and the real QTFs; and 5) motion of prong support junction that cannot be assumed completely fixed.[32] Our results clearly show that moving from the fundamental to the overtone mode, the quality factor increases for both QTF#1 and QTF#2. It can be concluded that air damping is the main losses mechanism affecting the vibrating tuning fork. According to Hosaka's model,[22] we expected $Q_{air,\,overt}/Q_{air,\,fund} \approx 2.91$ for both QTFs (see Table 2), while we measured an increase of the quality factor for the overtone mode of 2.58 and 2.48 with respect to the fundamental mode for QTF#1 and QTF#2, respectively. Hence, we can suppose that while the air damping effect decreases, the support loss mechanism starts to grow. In addition, QTF#1 exhibits an increase of the quality factor higher than that measured for QTF#2, in agreement with the support losses predicted by Hao's model (see Table 2).[26] Since the dissipation mechanisms are assumed independent of each other and the resonator quality factor is proportional to the inverse of total
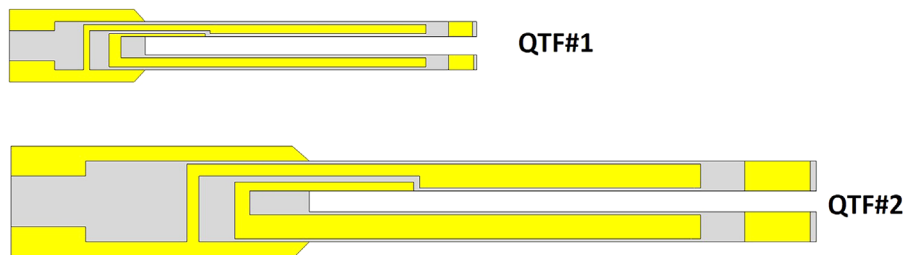

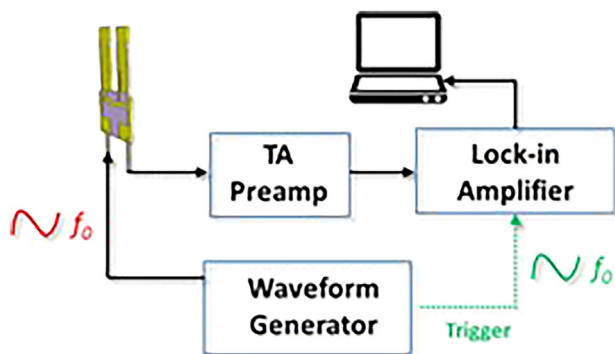**Figure 1.** Schematic view of the realized QTFs labelled as QTF#1 and QTF#2.

Figure 2. Schematic view of the experimental setup employed to electrically excite QTFs and acquire their frequency spectral response. TA – trans-impedance amplifier.

energy dissipated, the overall Q-factor can be calculated as a reciprocal sum of the two independent dissipative contributions:

$$\frac{1}{Q} = \frac{1}{Q_{\mathrm{sup}\,p}} + \frac{1}{Q_{\mathrm{air}}} \tag{5}$$

By using Q_{supp} and Q_{air} values listed in Table 1 for QTF#1 and QTF#2, the estimated quality factor values are: 10373 (QTF#1, fundamental mode), 2547 (QTF#1, first overtone mode), 6946 (QTF#2, fundamental mode), and 704 (QTF#2, first overtone mode). The combination of the Hosaka's and Hao's model predicts a reduction of the overall quality factor by a factor of 4.1 and 9.8 for QTF#1 and QTF#2, respectively, when moving from the fundamental to the first overtone mode. This

Table 3. Resonance frequencies and related quality factor values extracted from **Figure 3** for QTF#1 and QTF#2 fundamental and overtone modes, at atmospheric pressure.

	Fundamental mode		Overtone mode	
	f_0 [Hz]	Q-factor	f_1 [Hz]	Q-factor
QTF#1	3440.03	4400	21 415.19	11 370
QTF#2	2870.98	5860	17 747.47	14 570

is in contrast with our measurements. However, Q_{air} is supposed to increase when the first overtone mode is excited, as confirmed by the trend observed for the measured overall quality factors, for both QTFs. In order to reduce the contribution from air damping, the same analysis was performed at 25 Torr. The obtained response curves are shown in **Figure 4** and the obtained results are listed in **Table 4**. The overall quality factors are significantly higher with respect to those measured at atmospheric pressure, for both flexural modes. This further confirms that the vibrating prongs mainly suffer from air damping. Conversely, the model due to Hao predicts a huge contribution of support losses to the overall quality factor. At the first overtone mode, support losses are expected to increase more than one order of magnitude with respect to the fundamental mode, leading to a negligible contribution of Q_{air} in the overall quality factor estimation. This disagrees with our measurements, allowing to affirm that while the Hao's model well predicts the trend of the support losses as a function of the prong geometry, it overestimates the actual values. Indeed, for QTF #2 overtone mode, the estimated Q-
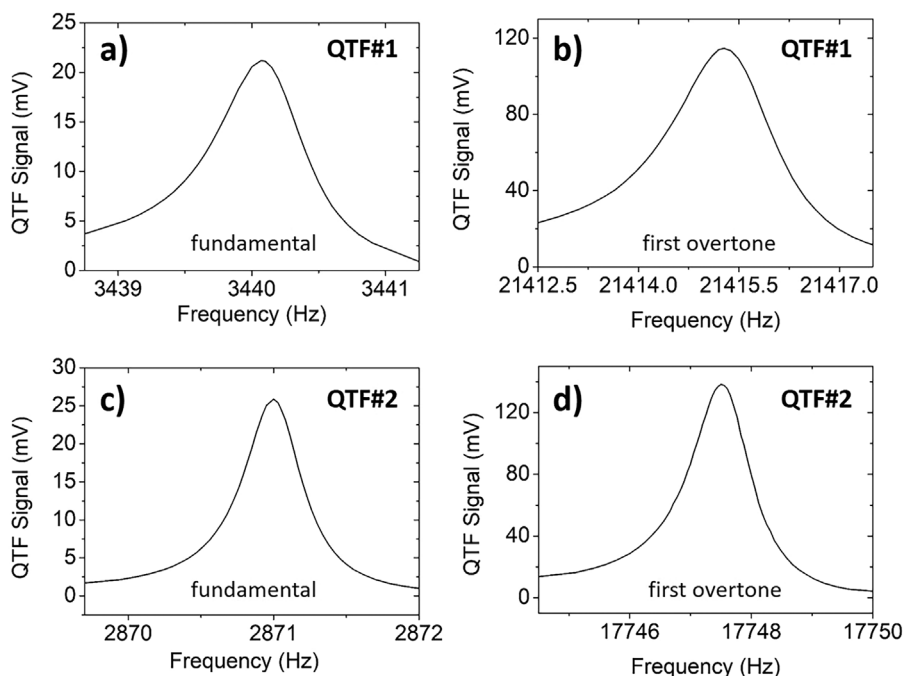

Figure 3. QTFs resonance curves measured at atmospheric pressure in standard air for QTF#1 fundamental (a) and first overtone mode (b), and for QTF#2 fundamental (c) and first overtone mode (d).
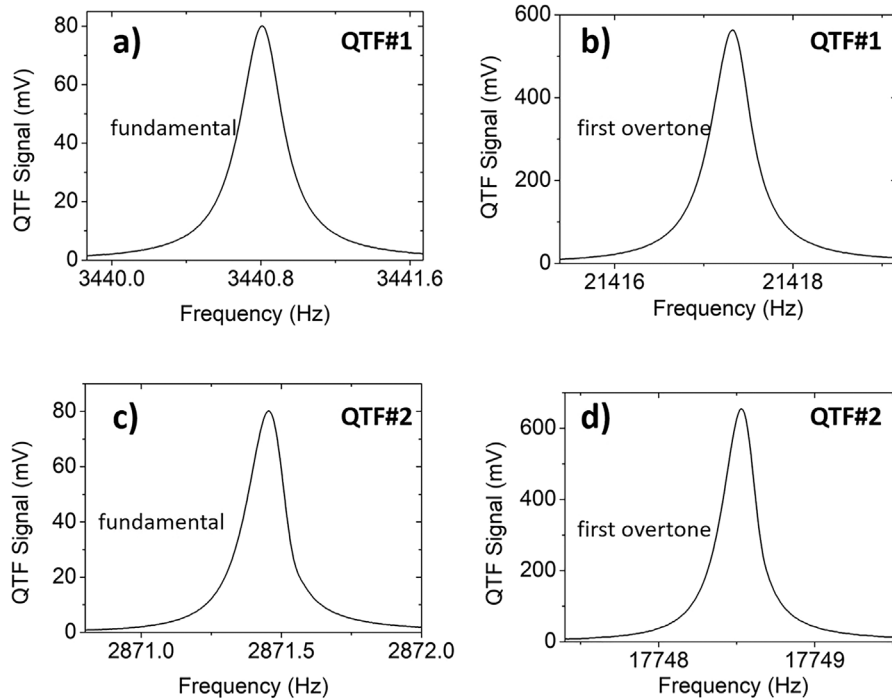
Figure 4. QTFs resonance curves measured at air pressure of 25 Torr for QTF#1 fundamental (a) and first overtone mode (b), and for QTF#2 fundamental (c) and first overtone mode (d).

factor is 704, while the observed value is $Q = 14570$ at atmospheric pressure and 65 730 at 25 Torr. With respect to the fundamental mode, QTF#1 exhibits a quality factor 3.78 times higher at the first overtone mode, while for QTF#2 this factor is 3.08. The discrepancy between these two factors is increased when the pressure is reduced, meaning that the support losses are not negligible. This effect is more evident in the QTF design showing the highest support loss value (QTF#1). Despite that, QTF#2 showed quality factors higher than those obtained for QTF#1, at both modes and pressure values, meaning that for the realization of QTFs with high Q-factors the air damping losses must be minimized. The effect of support losses can become remarkable at pressures much lower than 25 Torr, which is a pressure range typically not feasible for QEPAS operation.

5. Conclusion

In this work, we reported the performances of two QTFs designed to efficiently vibrate at the in-plane flexural

fundamental and first overtone modes, with a high quality factor. We identified two main loss mechanisms for in-plane flexural modes: air damping and support losses. Both mechanisms have been described as a function of the prong geometry and the vibrational mode. The investigated QTFs were designed to provide a resonance frequency of the fundamental mode falling around 3 kHz and a first overtone mode resonance around 20 kHz: with this choice, both modes are suitable for QEPAS operation. Among the possible prong geometries satisfying such requirement according to the Euler–Bernoulli equation, we selected two prong geometries differing in the theoretical contribution of the quality factor due to the air damping. The analysis of resonance properties has shown that the air damping is the dominant loss mechanism and it should be minimized when a specific resonance frequency is selected. Support losses become relevant at air pressures lower than 25 Torr, which typically is not a pressure range employed for QEPAS gas sensing applications.

Conflict of Interest

The authors declare no conflict of interest.

Table 4. Measured resonance frequencies and related quality factor values for QTF#1 and QTF#2 fundamental and overtone modes at a pressure of 25 Torr.

	Fundamental mode		Overtone mode	
	f_0 [Hz]	Q-factor	f_1 [Hz]	Q-factor
QTF#1	3440.81	11 820	21 419.14	44 680
QTF#2	2871.56	21 340	17 749.53	65 730

[1] R. Oria, J. Otero, L. Gonzalez, L. Botaya, M. Carmona, M. Puig-Vidal, *Sensors* **2013**, *13*, 7156.

[2] R. D. Grober, J. Acimovic, J. Schuck, D. Hessman, P. J. Kindlemann, J. Hespanha, A. S. Morse, K. Karrai, I. Tiemann, S. Manus, *Rev. Sc. Instr.* **2000**, *71*, 2776.

[3] F. J. Giessibl, *Appl. Phys. Lett.* **2000**, *76*, 1470.

[4] H. Gottlich, R. W. Stark, J. D. Pedarnig, W. M. Heckl, *Rev. Sci. Instrum.* **2000**, *71*, 3104.

[5] P. Patimisco, G. Scamarcio, F. K. Tittel, V. Spagnolo, *Sensors* **2014**, *14*, 6165.

[6] P. Patimisco, A. Sampaolo, H. Zheng, L. Dong, F. K. Tittel, V. Spagnolo, *Adv. Phys. X* **2016**, *2*, 169.

[7] P. Patimisco, A. Sampaolo, L. Dong, F. K. Tittel, V. Spagnolo, *Appl. Phys. Rev.* **2018**, *5*, 011106.

[8] M. Gonzalez, H. R. Seren, G. Ham, E. Buzi, G. Bernero, M. Deffenbaugh, *IEEE T. Instrum. Meas.* **2017**, *P99*, 1.

[9] D. Garg, V. B. Efimov, M. Giltrow, P. V. E. McClintock, L. Skrbek, W. F. Vinen, *Phys. Rev. B* **2012**, *85*, 144518.

[10] F. K. Tittel, A. Sampaolo, P. Patimisco, L. Dong, A. Geras, T. Starecki, V. Spagnolo, *Opt. Express* **2016**, *24*, A682.

[11] P. Patimisco, S. Borri, A. Sampaolo, H. E. Beere, D. A. Ritchie, M. S. Vitiello, G. Scamarcio, V. Spagnolo, *Analyst* **2014**, *139*, 2079.

[12] P. Patimisco, A. Sampaolo, L. Dong, M. Giglio, G. Scamarcio, F. K. Tittel, V. Spagnolo, *Sensor Actuat. B-Chem.* **2016**, *227*, 539.

[13] A. Sampaolo, P. Patimisco, M. Giglio, M. S. Vitiello, H. E. Beere, D. A. Ritchie, G. Scamarcio, F. K. Tittel, V. Spagnolo, *Sensors* **2016**, *16*, 439.

[14] H. Zheng, L. Dong, A. Sampaolo, P. Patimisco, W. Ma, L. Zhang, W. Yin, L. Xiao, V. Spagnolo, S. Jia, F. K. Tittel, *Appl. Phys. Lett.* **2016**, *109*, 111103.

[15] H. Zheng, L. Dong, P. Patimisco, H. Wu, A. Sampaolo, X. Yin, S. Li, W. Ma, L. Zhang, W. Yin, L. Xiao, V. Spagnolo, S. Jia, F. K. Tittel, *Appl. Phys. Lett.* **2017**, *110*, 021110.

[16] H. Wu, X. Yin, L. Dong, K. Pei, A. Sampaolo, P. Patimisco, H. Zheng, W. Ma, L. Zhang, W. Yin, L. Xiao, V. Spagnolo, S. Jia, F. K. Tittel, *Appl. Phys. Lett.* **2017**, *110*, 121104.

[17] P. Patimisco, A. Sampaolo, M. Giglio, V. Mackowiak, H. Rossmadl, B. Gross, A. Cable, F. K. Tittel, V. Spagnolo, *Opt. Lett.* **2018**, *43*, 1854.

[18] M. Christen, *Sensor Actuator.* **1983**, *4*, 555.

[19] Y. Jimbo, K. Itao, *J. Horological Inst. Jpn.* **1968**, *47*, 1.

[20] W. E. Newell, *Science* **1968**, *61*, 1320.

[21] F. R. Blom, S. Bouwstra, M. Elwenspoek, J. H. J. Fluitman, *J. Vac. Sci. Technol. B* **1992**, *10*, 19.

[22] H. Hosaka, K. Itao, S. Kuroda, *Sensor. Actuat. A-Phys.* **1995**, *49*, 87.

[23] K. Kokubun, H. Murakami, Y. Toda, M. Ono, *Vacuum* **1984**, *34*, 731.

[24] P. Patimisco, A. Sampaolo, V. Mackowiak, H. Rossmadl, A. Cable, F. K. Tittel, V. Spagnolo, *IEEE T. Ultrason. Ferr.* **2018**, *65*, 1951.

[25] D. M. Photiadis, J. A. Judge, *Appl. Phys. Lett.* **2005**, *85*, 482.

[26] Z. Hao, A. Erbil, F. Ayazi, *Sensor. Actuat. A-Phys.* **2003**, *109*, 156.

[27] J. A. Judge, D. M. Photiadis, J. F. Vignola, B. H. Houston, J. Jarzynski, *J. Appl. Phys.* **2007**, *101*, 013521.

[28] A. Sampaolo, P. Patimisco, L. Dong, A. Geras, G. Scamarcio, T. Starecki, F. K. Tittel, V. Spagnolo, *Appl. Phys. Lett.* **2015**, *107*, 231102.

[29] G. Wysocki, A. A. Kosterev, F. K. Tittel, *Appl. Phys. B* **2006**, *85*, 301.

[30] A. A. Kosterev, T. S. Mosely, F. K. Tittel, *Appl. Phys. B* **2006**, *85*, 295.

[31] Y. Ma, Y. He, L. Zhang, X. Yu, J. Zhang, R. Sun, F. K. Tittel, *Appl. Phys. Lett.* **2017**, *110*, 031107.

[32] D. M. Photiadis, D. J. Goldstein, J. M. Willey, *J. Appl. Phys.* **2016**, *119*, 064503.